Transactions, SMiRT-22
San Francisco, California, USA - August 18-23, 2013
Division V

Identification of Dynamic Characteristics of a Base-Isolated Building using Forced Vibration Tests

Masatoshi Okada[1], Hiroya Kouduru[2], Norio Taguchi[3], Minoru Koyama[3], Hiroshi Hibino[3] and Keisuke Kawamoto[1]

[1]Shikoku Electric Power Co., Inc., Japan (okada15164@yonden.co.jp)
[2]Yonden Consultants Co., Inc., Japan
[3]Taisei Corporation, Japan

ABSTRACT

Since the seismic behavior of a base-isolated building is strongly dependent on the mechanical properties of base-isolating devices, their performance verification is important from the point of view of the building's design and maintenance. This paper discusses the results of a study aimed at the identification of dynamic characteristics of an actual base-isolated building based on forced vibration tests using a couple of 30 kN shakers.

The testing structure is a seven-story base-isolated reinforced concrete building (located in an atomic power plant site), 32.4 m tall, and 51 m (E-W direction) × 21 m (N-S direction) in plan. A couple of eccentric mass shakers were installed on the roof of the building, and three force levels (frequency sweep from 0.3 to 8 Hz) were used. Through a comparison of the results of the forced vibration tests and microtremor measurements, the dynamic characteristics of the base-isolated building were identified using system identification analyses.

The following conclusions were made from the study: (1) Horizontal natural frequencies, damping ratios, and mode shapes of first and second modes were identified. (2) Reduction in natural frequencies and increase in damping ratios were observed with the increase in shaking moment. The changes in natural frequencies and damping ratios obtained from each test were significantly dependent on the displacement level of the base-isolation layer, examined from shear force-strain relations of the base-isolation layer and those of the superstructure. (3) A comparison of the shear force-strain relations of the base-isolation layer with the skeleton curve for small distortion obtained from a previous study revealed that the shapes of both curves corresponded well.

These results are utilized in the maintenance of base-isolating devices.

Keywords: seismic base isolation, forced vibration test, dynamic characteristics, lead-plugged rubber bearing

1. INTRODUCTION

The main service building at the Ikata Nuclear Power Plant, which has an emergency response room for initiating activities immediately after an earthquake or other emergent situations, has adopted a base-isolated structure. The appearance of the building is shown in Figure 1.

Since the seismic behavior of a base-isolated building is strongly dependent on the mechanical properties of base-isolating devices (rubber bearings, dampers, and so on), it is important to maintain a predetermined isolating function by means of a validity check of the design parameters, assumed conditions, and continuous maintenance of the isolating devices.

In general, the performance of a base-isolated building is guaranteed by the laboratory test data on the shear force-strain relation of each device. However, the dynamic characteristics of a real base-isolated building are rarely measured directly.

One of the methods for the direct measurement of the dynamic characteristics of an isolation building is the measurement of its free vibration caused by static enforced displacement with the application of loading devices such as hydraulic jacks.

However, the disadvantage of this method is that the isolation layer becomes stiffer with an increase in building size, resulting in the need for expanding the capability of hydraulic jacks according to the stiffness of the isolation layer. Moreover, this method requires the building of reaction blocks. For these reasons, it may be difficult to implement this test in a real building.

Hence, we tried to evaluate the fundamental vibration characteristics (such as natural frequencies, damping factors, and mode shapes) of the isolation building from the relation between excitation forces and responses, by using shakers installed on the building roof. This is comparatively easier than applying hydraulic loads. The results of this investigation are utilized as initial data for the maintenance of the building.

Figure 1: Appearance of testing building

2. OVERVIEW OF TESTING STRUCTURE

The testing structure is a seven-story, base-isolated reinforced concrete building that is 32.4 m tall, 51 m (E-W direction) × 21 m (N-S direction) in plan, and 143.5 MN in weight from the first floor to the top. The isolation layer is a combination of lead-plugged rubber bearings (LRBs), elastic slide bearings, and oil dampers. The schematic view of the isolation layer is shown in Figure 2.

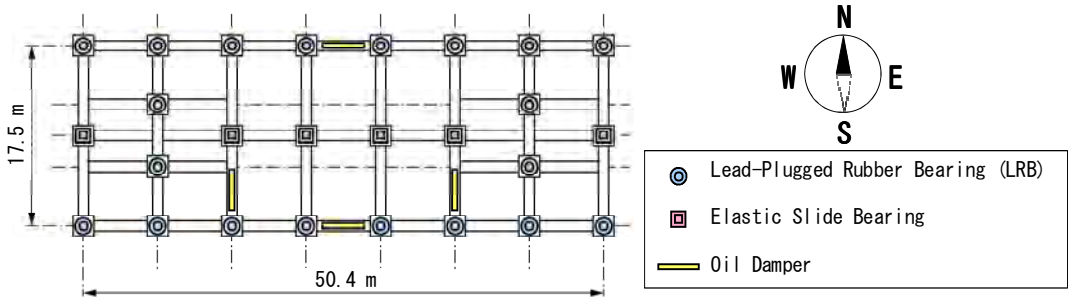

Figure 2: Schematic view of the isolation layer

3. TEST PLAN

A couple of eccentric mass shakers, each of whose shaking force is proportional to the square of the angular frequency of its weight, and with a maximum shaking force of 29.4 kN per set, were installed at both ends in the E-W direction of the building roof. Compulsive excitation by synchronized operation was performed.

These shakers were used for shaking in the following three cases:

1) E-W direction by coordinate phase;
2) N-S direction by coordinate phase; and
3) torsional direction by opposite phase.

The shaking for each case was subdivided into three steps of the total shaking moment: 1960 Nm, 784 Nm, and 196 Nm in E-W and N-S directions; and 1176 Nm, 588 Nm, and 196 Nm in the torsional direction. Table 1 lists the shaking moments with a logarithmic sweep from 0.3 to 8 Hz in the frequency range. Figure 3 shows the shaking force curves.

Figure 4 shows the distribution of vibration measuring points. These points were distributed across the base pit, the intermediate floors (1st, 3rd, 5th, and 7th), and the roof. The direction of measurement was changed corresponding to the shaking direction. The measuring station was placed on the 7th floor, and both the sensor signals and the phases of the shakers were transferred and recorded. Servo velocity meters were adopted for integrating the displacements with the amplifiers. The sampling frequency of the analog-to-digital converter was set up at 128 Hz. Moreover, microtremor measurements were also performed to compare their result with that of the shaking test.

Table 1: Shaking test plan

Case	Shaking Direction	Shaking Moment [Nm]	Frequency [Hz]	Shaking Term [min]
SX1	E-W	1960	0.3 to 2.0	20
SX2		784	0.5 to 3.0	17
SX3		196	1.0 to 6.0	12
SY1	N-S	1960	0.3 to 2.0	20
SY2		784	0.5 to 3.0	17
SY3		196	1.0 to 6.0	12
ST1	Torsional	1176	0.5 to 3.0	17
ST2		588	1.0 to 3.5	10
ST3		196	1.5 to 8.0	15

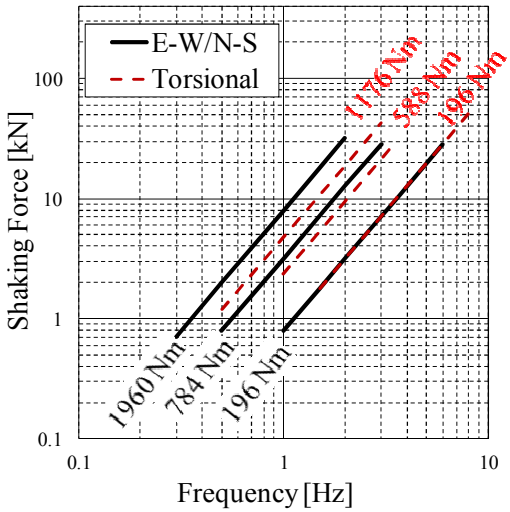

Figure 3: Shaking force curves

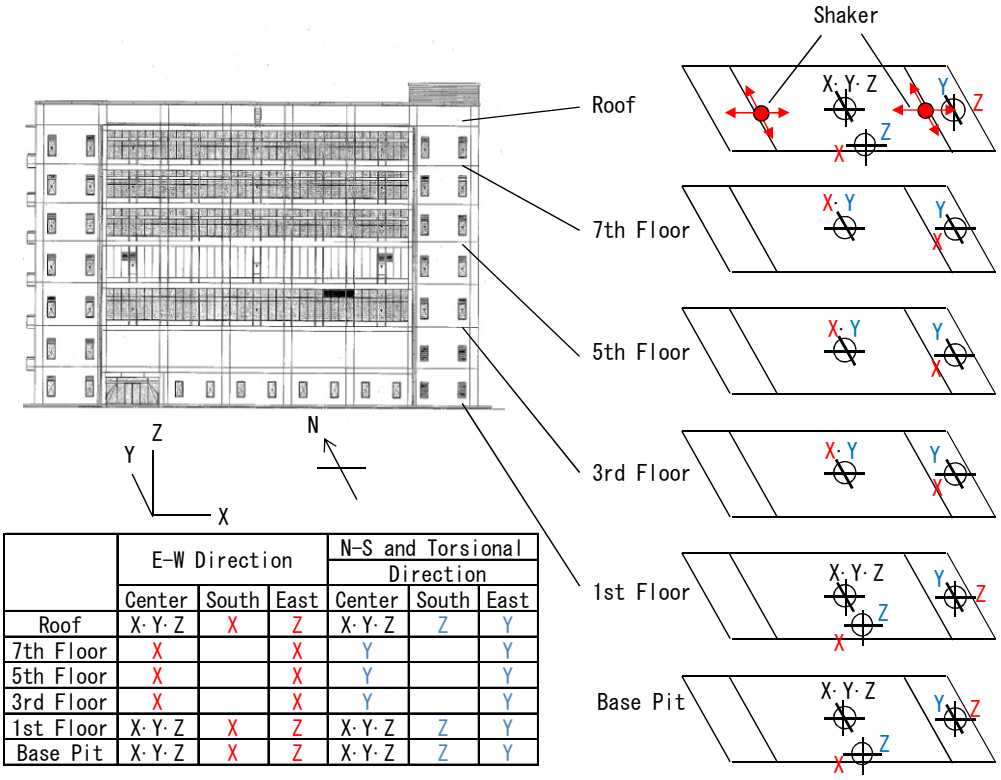

	E-W Direction			N-S and Torsional Direction		
	Center	South	East	Center	South	East
Roof	X·Y·Z	X	Z	X·Y·Z	Z	Y
7th Floor	X		X	Y		Y
5th Floor	X		X	Y		Y
3rd Floor	X		X	Y		Y
1st Floor	X·Y·Z	X	Z	X·Y·Z	Z	Y
Base Pit	X·Y·Z	X	Z	X·Y·Z	Z	Y

Figure 4: Distribution of vibration measuring points

4. RESULTS OF TESTS

4.1 Microtremor Measurements

Displacement transfer functions were calculated in the E-W and N-S directions by using datasets of microtremor measurements of the testing building. Figure 5 shows the displacement transfer functions between the base pit and the evaluated measuring points (1st and 5th floors, and the roof), which were chosen along the centerline of the building. In addition, the figure shows the red curves made to fit the transfer functions. Table 2 lists the natural frequencies obtained from the fitted curves. Although the transfer functions are not shown here, the peak frequencies (observed only on the east side) were estimated to be in the torsional modes, shown in the table within parentheses.

Table 2: Natural frequencies and damping ratios obtained from shaking tests and microtremor measurements

		1st Mode				2nd Mode	
Shaking Moment		1960 Nm	784 Nm	196 Nm	Microtremor	196 Nm	Microtremor
E-W	Frequency [Hz]	1.788	1.825	1.888	1.985	4.488	4.768
	Damping Ratio [%]	4.09	2.93	2.41	1.66	2.73	1.23
N-S	Frequency [Hz]	1.655	1.693	1.736	1.811	4.743	4.975
	Damping Ratio [%]	3.60	2.56	2.27	2.47	2.00	0.24
Shaking Moment		1176 Nm	588 Nm	196 Nm	Microtremor	196 Nm	Microtremor
Torsional	Frequency [Hz]	2.158	2.198	2.252	(2.35)	6.606	(near 7)
	Damping Ratio [%]	4.09	2.93	2.66	-	2.35	-

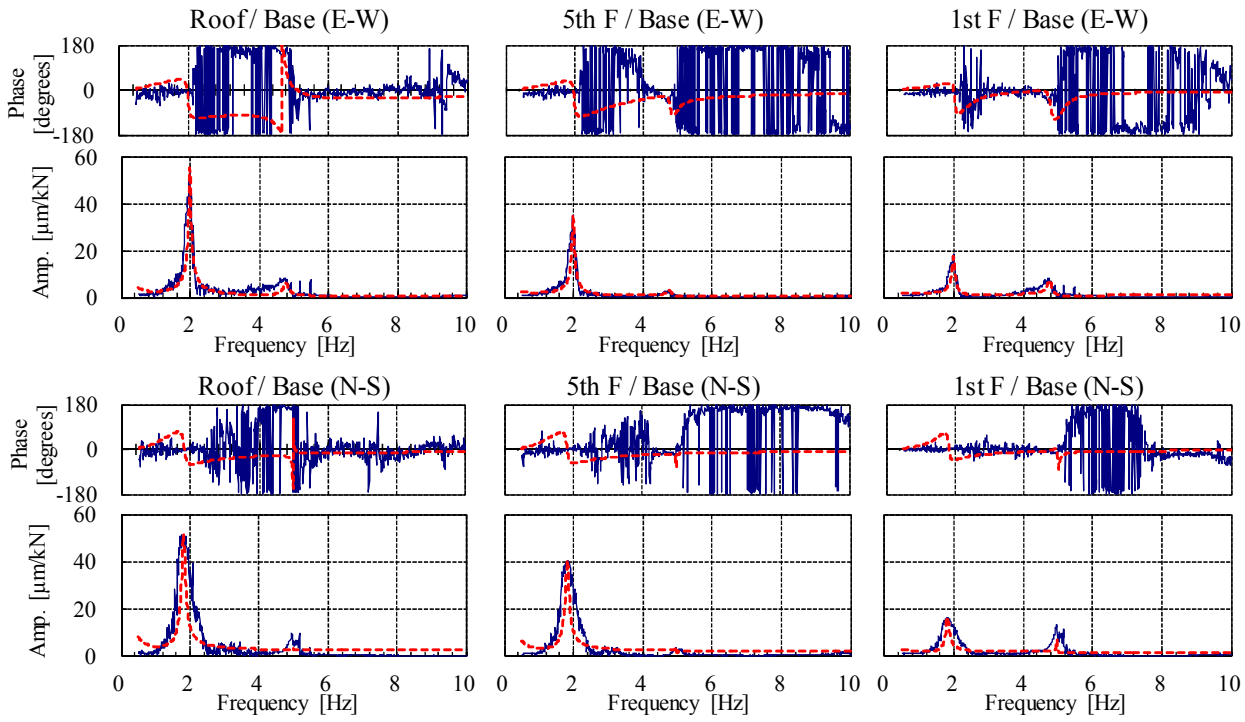

Figure 5: Transfer functions calculated from microtremor measurements

4.2 Forced Vibration Tests

Figure 6 shows the transfer functions between the base and the measuring points (1st floor and the roof) obtained in the case of the 196 Nm shaking moment, with the red curve made to fit the transfer functions. In addition, Table 2 gives the first and second frequencies and damping factors for each case of shaking. From a comparison of the transfer functions of the shaking tests with those of microtremor measurements, the peaks of the natural frequencies in the shaking tests are clear. The observation of strain-amplitude dependence reveals that in the first mode, the natural frequency in each direction fell gradually with the increase in shaking moment. Compared to the results of microtremor measurements, the natural frequencies decreased to about 95% in the case of the 196 Nm shaking moment. Moreover, an upward tendency in damping ratios is also observed with an increase in shaking moment. Figure 7 shows the mode shapes in each direction in the case of the 196 Nm shaking moment.

The first mode does not show where the deformation gathered around the isolated layer but shows that the isolated layer deformed greatly and was accompanied by superstructure deformation. The shapes of the second mode indicate that the isolated layer deformed significantly with a node around the 5th floor. The maximum displacement was about 130 μm on the 1st floor and 350 μm on the roof, in both in the E-W and N-S directions. In the case of isolated layer displacement on the 1st floor is about 130 μm, the shear strain was negligible (0.07%) for LRB (total thickness of rubber being 198 mm) and was 0.29% for elastic slide bearings (total thickness of rubber being 45 mm). Since the shear forces that acted on the elastic slide bearings used in the tests were less than the static friction forces, slide had not occurred in elastic slide bearings.

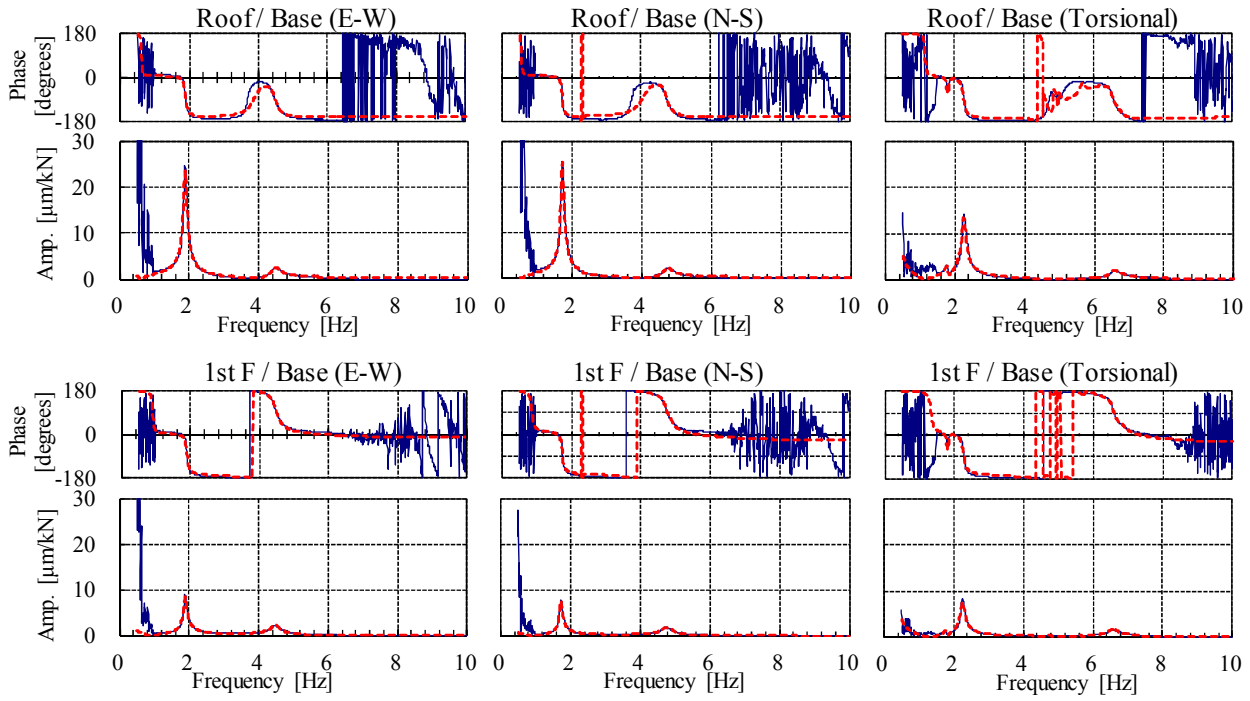

Figure 6: Transfer functions calculated from shaking tests

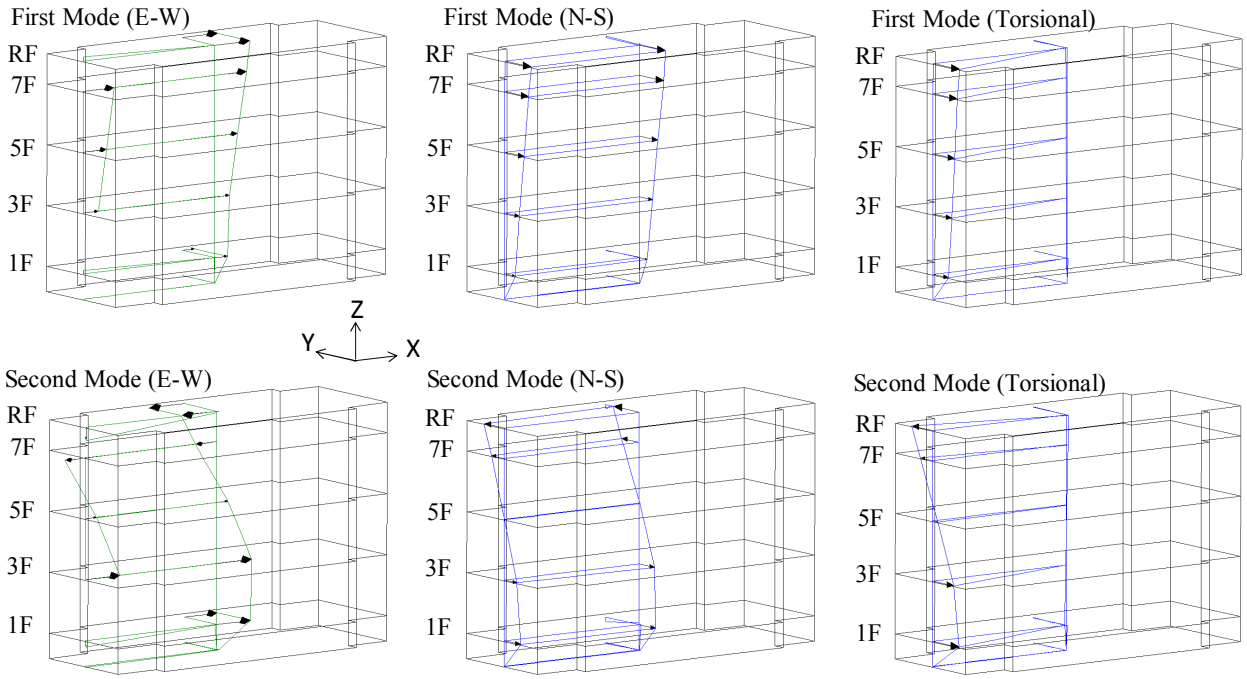

Figure 7: Mode shapes in each direction

5. EVALUATION OF ISOLATED LAYER STIFFNESS

5.1 Strain-Amplitude Dependence

A decrease in natural frequencies and increase in damping ratios were observed with the increase in shaking moment. The above phenomena were examined to understand the strain-amplitude dependence on the isolated layer stiffness or on the superstructure (such as concrete) stiffness. In the case of a lumped mass model as shown in Figure 8, when the shaking force f is acting on the roof, using the equation of motion, the stiffness of the nth layer can be derived as

$$k_n = \frac{f - \left(m_1\ddot{x}_1 + m_2\ddot{x}_2 + \cdots + m_n\ddot{x}_n\right)}{\left(x_n - x_{n+1}\right)} \tag{1}$$

where m is the mass, k is the stiffness, and x is the displacement of each layer. Since the measuring points were only on the odd floors, the mass of the even floor was distributed to the upper and lower floors each by one-half. With each shaking moment, one cycle was selected where the peak amplitude of the 1st natural frequency appears. Figure 9 shows the result of the evaluated shear force-deformation relations of the base-isolation layer and of the superstructure. The figure also shows the damping factors calculated from the area of one cycle of the hysteresis loop, as well as the straight line connecting the positive/negative peak of deformation. Shear force-deformation relations of the base-isolation layer are almost linear and the area of the loops is small when the shaking moment is 196 Nm. However, the loop area increases and the slope (stiffness) decreases with increase in the shaking moment. The loop area is maximum and the slope is minimum at a shaking moment of 1960 Nm. On the other hand, regardless of the level of shaking moment, the shear force-deformation relation of the superstructure is mostly linear and the layer stiffness is also almost constant. The stiffness of the isolation layer in the case of the 1960 Nm shaking moment in the E-W direction decreased to 84.4% of that in the case of 196 Nm moment. The damping factor of the isolated layer evaluated from the hysteresis loop was 2.7% and 7.3% in the cases of the 196 Nm and 1960 Nm moments, respectively; on the other hand, that of the superstructure was correspondingly 0.3% and 0.7%, respectively, indicating that the increase in the damping factor of the superstructure was quite negligible. As mentioned above, it is presumed that the change in natural frequency and damping factor with the shaking moment is significantly influenced by the strain-amplitude dependence of the isolation layer and minimally influenced by the superstructure.

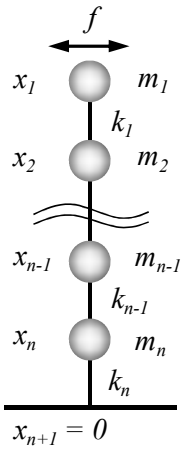

Figure 8: Lumped mass model

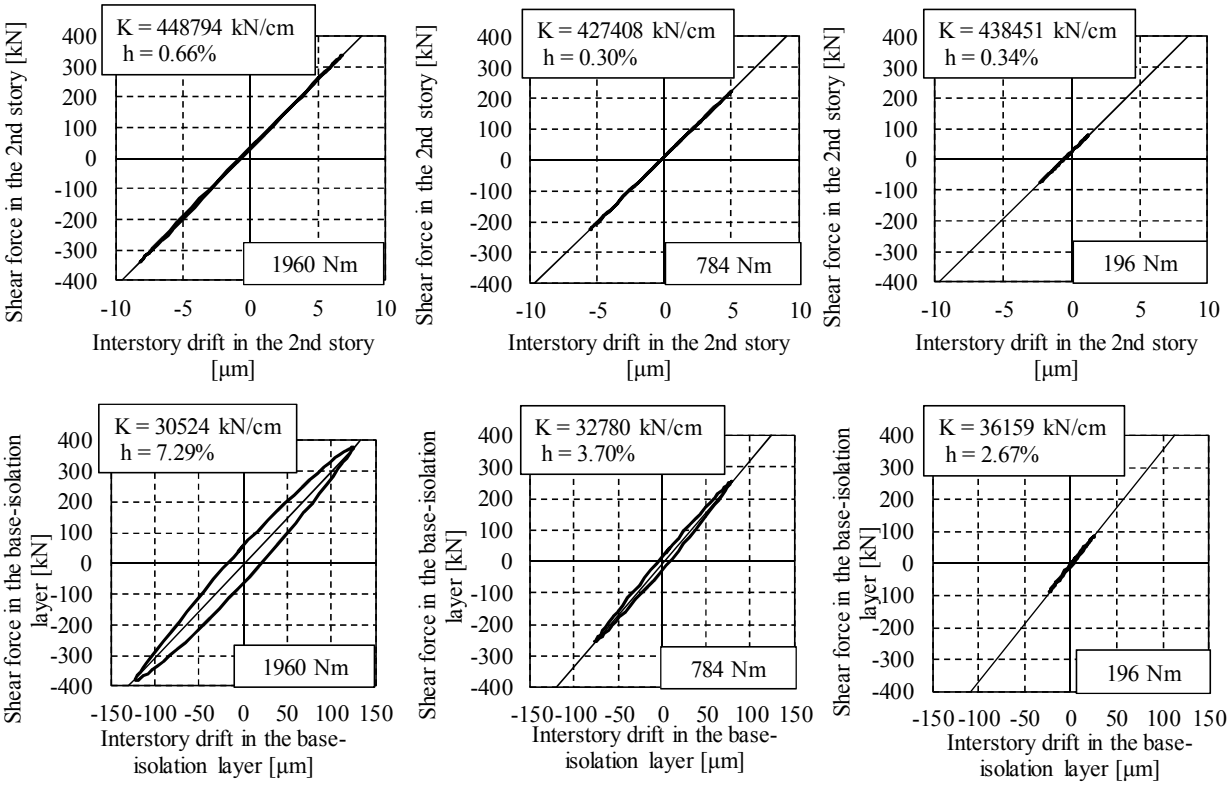

Figure 9: Shear force-deformation relations (E-W direction)

5.2 Comparison with Design Stiffness

The above result is compared with the design horizontal stiffness. As the hysteresis model of LRB, the "modified H-D model[1)]" was used in the design. It is one of the models that can express the hysteresis curves of laminated rubber bearings more accurately than can bilinear models, with the feature of its stiffness of return from post–yield stiffness, *Ke*, being equal to the initial stiffness of the minute amplitude. The study in reference 1) indicates that when the stiffness of rubber without plugged lead is 120 times lower than *Ke*, it shows the obtained results are in good agreement with those obtained by the loading test. In the hysteresis model of elastic slide bearings, a bilinear model having initial stiffness of rubber and the post-yield stiffness after slide exceeding the static friction was used in the design. The sum of the initial stiffnesses is 29,228 kN/cm (*Ke* accounts for 99.2% of initial stiffness). In the case of the 196 Nm shaking moment, in which the strain was the smallest and stiffness was high, the stiffness of the isolation layer was 36,159 kN/cm, which is about 24% higher than the designed value. Since shear force-deformation relations show nonlinear loop curves even at the 196 Nm shaking moment, the stiffness must increase from that under the influence of strain-amplitude dependence in very minute deformations.

Next, the force-deformation relations obtained from this study were compared with the example that examined the hysteresis of LRB under small strain. LRB has a feature that shows the elastic-plastic hysteresis loop from a very small strain zone. The study in reference 1) examined the force-deformation relation at the time of small strain, based on the incremental displacement amplitude cyclic loading test with 10% or less shear strain, and showed that experimental hysteresis loops were well simulated by expressing the skeleton curve of rubber shearing strain (0.1% to 10%) using an exponential function. Figure 10 shows the maximum deformation under the shear force-deformation relations of the isolation layer without elastic slide bearings at the time of each shaking moment. It also shows that the skeleton

curve of LRB (based on the study in reference 1)) was set up at first from the LRB maker's design curve[2)] in the rubber shearing strain range of 10% to 250%. Next, the expression of the relations (shearing force $Q = a\gamma^{0.6}$) of the exponential function proposed by the study in reference 1) was used for the shear strain range of 0.1% to 10%. The coefficient a was determined to be the point at which both skeleton curves would connect at 10% shear strain. Figure 10 also shows the skeleton curve after considering the scattering in rubber characteristics because of real design factors such as manufacturing, environmental temperature, and aged deterioration. It can be concluded that the curve with the tendency of a straight line on a log-log axis indicates a good correspondence relation, although the stiffness from the test shows slightly higher values than that from the extended skeleton curve (of reference 1)) at the time of small strain.

In addition, incidents such as the contact with the exterior, pipes at the base pit, and the restraint of dampers (deformation being too minute and dampers not moving) may alter the stiffness in small amplitude during the shaking tests, causing the evaluated stiffness to be excessive.

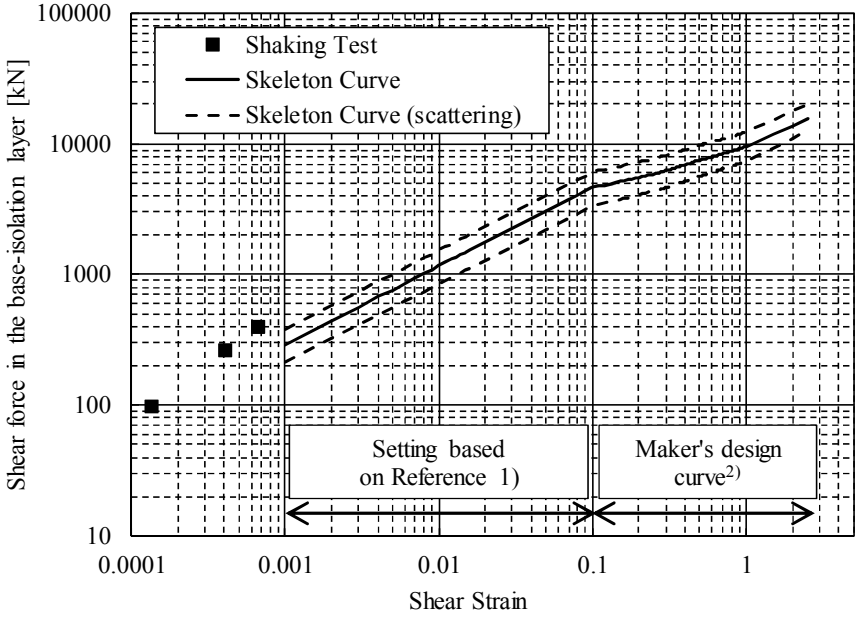

Figure 10: Skelton of base-isolation layer

6. MAINTENANCE OF BASE-ISOLATING DEVICES

The results obtained by the tests in this study are considered as initial data in the maintenance of base-isolating devices. The change in vibration characteristics was monitored using a seismograph installed in the building. Moreover, the same shaking tests will be carried out periodically if necessary, and the change in the stiffness, the damping of the isolation layer, and the strain-amplitude dependence will be measured.

7. CONCLUSION

The results of the shaking tests and the microtremor measurements lead us to the following conclusions. These results are utilized for the maintenance of base-isolating devices.

(1) Horizontal natural frequencies, damping ratios, and mode shapes of first and second modes were identified.

(2) The shape of the first mode does not indicate that only the isolated layer deformed without superstructure deformation; however, the isolated layer deformed greatly and was accompanied by superstructure deformation. The second mode shape indicates that the isolated layer deformed significantly with a node around the 5th floor. The maximum deformations in peak frequencies were observed on the 1st floor.

(3) The maximum displacement of the isolated layer was about 130 μm (the shear strains of LRB and elastic slide bearings were 0.07% and 0.29%, respectively) and the maximum displacement at the roof was about 350 μm.

(4) A decrease in natural frequencies and increase in damping ratios were observed with the increase in shaking moment. From shear force-deformation relations of the base-isolation layer and of the superstructure, the change in natural frequencies and damping ratios obtained for each test was found to be significantly dependent on the strain level of the base-isolation layer.

(5) The stiffness of the isolation layer during shaking tests with a shaking moment of 196 Nm was 24% higher than the initial stiffness of the design. Comparison with the example that considered the skeleton curve of LRB at the time of small strain revealed that although the stiffness of the isolation layer in the shaking tests tended to be greater, the curve profile showed a harmonic tendency.

REFERENCES

1) Takenaka, Y., Yamada, K. and Yoshikawa, K. (2001). “Modified H-D model: a new smooth-curve hysteresis model of laminated rubber bearings for base isolation (In Japanese)” *AIJ J. Technol. Des.* No.14, 87-92.
2) Technical Documents for Lead-Plugged Rubbers (2008) Bridgestone Corporation.
3) Okada, M., Kouduru, H., Taguchi, N., Koyama, M., Hibino, H. et al. (2012). “Forced vibration test of base-isolated building at the Ikata Nuclear Power Station Part 1-3 (In Japanese)” *AIJ Summaries of Technical Papers of Annual Meeting.* Structure II, 223-228.